Article

Elucidation of the roles of Re in aqueous-phase reforming of glycerol over Pt-Re/C catalysts

Zhehao Wei, Ayman M. Karim, Yan Li, and Yong Wang

ACS Catal., **Just Accepted Manuscript** • DOI: 10.1021/acscatal.5b01770 • Publication Date (Web): 27 Oct 2015

Elucidation of the roles of Re in aqueous-phase reforming of glycerol over Pt-Re/C catalysts[#]

Zhehao Wei[a,b†], Ayman Karim[b‡*], Yan Li[a], Yong Wang[a,b*]

[a] The Gene and Linda Voiland School of Chemical Engineering and Bioengineering, Washington State University, Pullman, WA 99164, USA

[b] Institute for Integrated Catalysis, Pacific Northwest National Laboratory, Richland, WA 99352, USA

ABSTRACT: We report the investigation of surface properties of Pt/C and Pt-Re/C catalysts using *in situ* spectroscopic tools and the fundamental understanding of their catalytic performances in glycerol aqueous-phase reforming (APR). We found that adding Re to Pt/C improves its activity significantly, which is consistent with our previous observation in glycerol steam reforming. However, the difference in reaction selectivity is much more pronounced in APR. Compared to Pt/C, Pt-Re/C yielded significantly more liquid products, while the selectivity to H_2 and CO_2 decreased by more than 40%. In-operando X-ray absorption spectroscopy and attenuated total reflectance infrared (ATR-IR) with *in situ* capability as well as Raman spectroscopy were employed to investigate the catalyst surface properties and the roles of Re. In-operando X-ray absorption fine structure (XAFS) shows significant oxidation of Re, and ATR-IR of adsorbed pyridine revealed the formation of acid sites on PtRe after hot liquid water treatment. Additionally, ATR-IR using CO as probe molecule demonstrated that CO desorption from the Pt-Re/C surface is more facile than that from Pt/C in aqueous phase. We propose that well-dispersed Re oxide species in close proximity with Pt work as the active site providing both metal and acid functionalities while the terminal Re-O moiety has little contribution to the overall reactivity as evidenced by Raman spectroscopy.

KEYWORDS: aqueous-phase reforming, bimetallic catalyst, platinum-rhenium, rhenium oxide, catalysis in condensed water, surface acidity, selectivity, in situ and in-operando spectroscopy

[#] Invited submission to the ACS Catalysis special issue on Catalysis at U.S. Department of Energy National Laboratories

Received on 08/12/2015
Revised on 10/12/2015 and 10/22/2015
Accepted on xx/xx/xxxx

1. Introduction

Glycerol has been reported to be a good model compound in biomass catalytic conversion, with functionality that benefits the mechanistic understandings. Cortright et al.[1] first confirmed the feasibility of performing glycerol aqueous-phase reforming (APR) with high hydrogen yield using a benchmark Pt/Al_2O_3 catalyst. Wen et al. screened a few catalysts and came up with the order of hydrogen production rate, in terms of active metal, of Pt > Cu > Ni > Co[2]. Extensive research has confirmed that adding a second metal (e.g., Mo[3, 4], Ni[5, 6], or Re[7-12]) to Pt catalysts can enhance the catalytic activity, and some new insights into the role of these second metals have also been proposed. Dietrich et al.[4] observed 4 times higher turnover frequency (TOF) over PtMo/C and higher selectivity to C-O bond cleavage than that over Pt/C, and ascribed the role of Mo to altering the electronic properties of Pt, lowering the binding energy of CO and reducing the activation energy of both dehydrogenation and C–O bond cleavage. In-operando characterization indicated that the catalyst surface is mainly composed of Pt-rich bimetallic PtMo nanoparticles and oxidized Mo[3]. We compared the performances of Pt/C and Pt-Re/C catalysts in glycerol APR and found a higher TOF of about one order of magnitude over Pt-Re/C, along with higher selectivity to dehydration products over Pt-Re/C[8]. *In situ* characterizations using X-ray photoelectron spectroscopy (XPS) and ammonia temperature programmed desorption (NH_3-TPD) confirmed that Re becomes oxidized, creating surface acidity upon hydrothermal treatment (in this case steam treatment); the concentration of acid sites was found to increase with Re addition, favoring C–O over C–C cleavage while hydrogen selectivity was decreased[10]. However, the effect of liquid phase hydrothermal conditions on the catalyst structure is still not well understood. Therefore, it is worthwhile to separately investigate these two cases, i.e., vapor phase steam and aqueous phase. Our most recent investigation[12] on steam treatment of Pt-Re catalyst and its performances in steam reforming of glycerol indicated that upon steam treatment, oxidized Re species could facilitate CO spillover and desorption from neighboring Pt sites, making them accessible to glycerol reactant, and leading to the overall enhanced activity while selectivity to products remains the same.

In the present work, we extend our studies to elucidating the roles of Re on Pt-Re/C bimetallic catalyst in aqueous phase reforming of glycerol. We particularly focus on understanding the effects of water phase (i.e., condensed phase vs vapor phase) on the structure and surface properties of Pt-Re, and correlating these properties with catalyst activity and selectivity in glycerol APR reaction. *In situ* techniques such as X-ray absorption fine structure (XAFS), attenuated total reflectance infrared (ATR-IR), and Raman spectroscopy are used to characterize Pt/C and Pt-Re/C catalysts to help understand their properties under reaction conditions.

2. Experimental

2.1. Catalyst preparation

The catalyst preparation procedure has been reported previously[12]. Briefly, active carbon support (TA 60, PICATAL, 60~100 mesh) was dried at 110 °C overnight prior to use. Tetraammineplatinum(II) nitrate hexahydrate ($(NH_3)_4Pt(NO_3)_2 \cdot 6H_2O$, 99.999%, Sigma-Aldrich) and perrhenic acid ($HReO_4$, 99.99%, in 65-70% aqueous solution, Sigma-Aldrich) were used as metal precursors. Pt/C and Re/C were prepared by incipient wetness impregnation. The impregnated samples were dried at 110 °C for 2 h and calcined at 260 °C for another 2 h. Bimetallic Pt-Re/C was prepared by impregnating Re precursor solution onto the calcined Pt/C sample followed by the same drying and calcination steps.

2.2. Catalyst characterization

Attenuated total reflectance infrared (ATR-IR) characterization of the samples was performed using a home-made ATR cell with the details previously reported[12]. The catalyst sample was ground into fine powder and suspended in nanopure water under sonication to form an ink. This ink was then coated onto the round top surface of the IRE and dried overnight to form a thin layer. The ATR cell can be heated to up to 300 °C by a cartridge heating element integrated with a Watlow temperature controller. A HPLC pump (LabAlliance Series III) was used to deliver pressurized liquid into the cell. A backpressure regulator (BPR, KPB1L0A412P20000, Swagelok) was used to control the system pressure downstream.

The sample was reduced in 10% H_2/Ar (10 mL/min) from room temperature to 280 °C at 5 °C/min. After 1 h reduction, the gas was switched to 10 mL/min He and purge for 10 min before cooling down. The sample was held at room temperature for at least 10 min before collecting a background spectrum. 10 mL/min 1% CO/He was then introduced and a series of sample scans were taken every minute. The resolution of each scan was set at 4 cm^{-1} and 128 scans were averaged to generate each spectrum. For the CO desorption measurement as a function of temperature, a series of spectra under He at 200, 150, 100, 50 and 25 °C were collected before introducing CO and used as the background spectra for the desorption counterparts. For experiments requiring high pressure liquid environment, liquid was delivered by the HPLC pump at a certain flow rate (typically 0.1 mL/min if not otherwise specified; catalyst layer was intact following high pressure water flow) after the cell was pressurized with N_2 and the backpressure set at 450 psi by the BPR. CO adsorption under liquid environment was performed by co-feeding CO with liquid water (0.01 mmol CO/L H_2O). CO desorption was carried out by switching to pure water flow. The IR data collected in the presence of liquid water was corrected by subtraction of a scaled water background spectrum according to a procedure described elsewhere[13].

Raman spectra of the catalyst samples were collected with a Horiba LabRAM HR Raman microscope system reported before[14]. The system is equipped with a 532 nm laser source (Ventus LP 532) and a Synapse CCD (charge coupled device) detector. Catalysts were loaded in an *in situ* reaction cell (Linkam CCR1000) for Raman characterization. Sample reduction was carried out under 10% H_2/Ar (20 mL/min) at 280 °C for 1 h. For those requiring hot liquid water (HLW) exposure, the samples were first treated in a batch reactor in the similar manner (hydrogen reduction followed by exposure to water at APR reaction condition without feeding glycerol) as described in section 2.3. After 2 h, the catalyst samples were collected and immediately transferred to the reaction cell under N_2 protection to minimize exposure to air. The samples were then dried under He flow (20 mL/min) at 110 °C for 2 h.

The catalysts were probed by X-ray absorption spectroscopy (XAS) in transmission mode using an in-house built in-situ cell rated to 1100 psi and 700 °C, as previously reported [12,

15]. It consists of a flow reactor and the cell body made of stainless steel and heated by resistive heating cartridges. An X-ray window (1 cm horizontal × 0.5 cm vertical) allows for measurements in transmission mode. The catalyst bed (about 60 mg, 60~100 mesh) was packed with quartz wool on both ends in a glassy carbon tube (o.d. = 6.35 mm, i.d. = 4.1 mm, from HTW Hochtemperatur-Werkstoffe GmbH, Germany). and connected to the rest of the system via standard Swagelok fittings using graphite ferrules (450 °C temperature rating). The reaction temperature was controlled using a Watlow temperature controller within ±1 °C, measured on the external tube wall using a K type thermocouple. The XAS measurements were performed at beamline X-18A at the National Synchrotron Light Source (NSLS) operated by the Synchrotron Catalysis Consortium (SCC) at Brookhaven National Laboratory (BNL). The measured Pt and Re absorption edge steps for Pt and Re for the catalysts were about 0.65.

X-ray absorption near edge structure (XANES) and Extended X-ray absorption fine structure (EXAFS) data processing and analysis were performed using Athena and Artemis programs of the IFEFFIT data analysis package[16, 17]. Three scans were collected under each condition and merged after alignment using Pt (or Re) foil spectrum collected simultaneously for each scan. Scans were collected at the Pt $L_{2,3}$ and Re L_3 edges. For the Pt-Re catalyst, due to the overlap of the Re L_2 (11959 eV) with the Pt L_3 (11564 eV) which limits the EXAFS signal to 9.6 Å-1 in k-space, we collected the EXAFS signal at the Pt L_2 edge which extends the k-range to 12.1 Å-1. $\chi(k)$ (where k is the photoelectron wavenumber) was obtained by subtracting smooth atomic background from the normalized absorption coefficient using the AUTOBK code. The theoretical EXAFS signal was constructed using the FEFF6 code and fitted to the data in r-space using the Artemis program of the IFEFFIT package. The spectra were fitted in r-space by varying the coordination number (CN) of the single scattering Pt–M (Re–M or Re-O) path, the bond length disorder (Debye–Waller factor), σ^2, the effective Pt–M (Re-M or Re-O) scattering length, and the correction to the threshold energy, ΔE_0. S_0^2 (passive electron reduction factor) was obtained by analyzing the spectrum for Pt and Re foils, and the best fit value (0.93 for Pt L_2, and 0.86 for both Pt L_3 and Re L_3) was fixed during the fitting of the catalyst samples. The values for S_0^2 are consistent with our previous work[5, 15] and values reported in the literature[18, 19]. Re consisted of Pt-Re/C sample contained a mixture of metallic Re and ReOx and fitting the spectra to a single Re-O scattering path did not result in good fits. We used a similar model to the one proposed by Bare et al.[18] for Re/Al_2O_3 where they used two Re-O scattering paths at about 1.73 Å and 2.08 Å. The model with two Re-O scattering paths gave a much better statistical fit (reduced χ^2 was lower by a factor of 5-10) than the model with a single Re-O scattering path. The k-range used for Fourier transform of the $\chi(k)$ was 2.5–12 Å-1 for Pt and 2.5-13.9 Å-1 for the Re edge and the r-range for fitting was 1.8–3.3 Å for Pt and 1.1–3.2 Å for Re unless otherwise specified.

2.3. Catalyst evaluation in batch reactor for glycerol APR

The catalyst sample was ground and sieved to 325~400 mesh before loading into the reactor for evaluation. A 50 mL micro stirred reactor purchased from Parr Instrument was used for this study. Typically, after the charge of a certain amount of catalyst, the reactor was flushed with Ar to remove air. Then it was pressurized with 10% H_2/Ar and depressurized for three times before a final pressurization to 20 psi. After the catalyst was *in situ* reduced at 280 °C for 1 h and cooled down to room temperature, the gas inside was vented and 20 mL 10% glycerol aqueous solution was injected into the vessel by a syringe without opening or exposing the reduced catalyst to air. After pressurizing and depressurizing the reactor with N_2 for three times to remove residual H_2/Ar, a final charge of N_2 to 80 psig was applied. The mixture was stirred at 300 rpm for 10 min before heating; after reaching the reaction temperature, the reaction was run under vigorous stirring at 600 rpm for 2 h before quenching the reactor vessel in an ice bath. The inner pressure at 225 °C reached above 450 psi, as typically required for APR reaction. Under such reaction conditions, no significant mass transfer limitation is observed (i.e., no change in activity at a higher stirring rate or smaller catalyst particle size). Product analysis followed the same procedure reported before[12]. Briefly, the gas products were collected in a Tedlar gas bag (1 L, Sigma-Aldrich) and analyzed offline with an Agilent 490 micro GC equipped with four independent modules (a molsieve column, a CP-PoraPLOT U column, an aluminum oxide column, and a CP-Sil 5CB column, all with TCDs; the molsieve used Ar as reference gas while all other modules used He). After depressurizing and opening the vessel, liquid product was separated from solid catalyst by a 0.2 μm syringe filter and analyzed using a Waters Breeze 2 HPLC equipped with a Bio-Rad Aminex HPX-87H ion exclusion column (300 mm × 7.8 mm) and a refractive index detector. The mobile phase was 5 mM H_2SO_4 aqueous solution at a flow rate of 0.6 mL/min. The carbon balance is generally higher than 90%.

3. Results and discussion

3.1. Catalytic reactivity in glycerol aqueous-phase reforming

Batch reaction of glycerol APR was carried out over Pt/C and Pt-Re/C catalysts. The catalyst loading (50 mg of 3%Pt/C and 20 mg of 3%Pt-3%Re/C) was varied to obtain similar glycerol conversion (around 15%). The turnover frequency (TOF) was calculated as either the consumption rate of glycerol or the formation rate of each product divided by the Pt dispersion measured in our previous report using the same catalysts[12]. We also note here that APR reaction is known to be catalyst structure sensitive[20]. However, the Pt particle sizes in this study are mostly 1~2 nm as we previously observed[10]. According to Kirilin et al.[20], within this narrow particle size range the catalyst structure sensitivity for APR reaction is negligible.

As we have previously reported[8, 10], the catalytic performances of Pt/C and Pt-Re/C in glycerol APR reaction are significantly different. Glycerol TOF is more than 5 times higher over 3%Pt-3%Re/C than over 3%Pt/C, as can be seen in Figure 1. Similar enhancement in catalytic activity with addition of Re to Pt/C has been reported before[7, 8, 10-12]. Additionally, the product distributions are significantly different. As shown in Table 1, the value X_G/X_L, representing the ratio between conversion to gas products and liquid products, was 0.9 for 3%Pt/C and 0.4 for 3%Pt/-3%Re/C, indicating that production of liquid products was more facile over Pt-Re/C. From the results shown in Figure 1, it can be observed that the addition of Re causes a significant shift from the production of the gas

products H_2 and CO_2 to the production of the liquid products, such as acetol and ethanol.

Table 1 Glycerol APR over Pt and Pt-Re catalysts supported on active carbon (reaction temperature 225 °C, operated at initial pressure at room temperature of 80 psi N_2); catalysts were *in situ* reduced under 20 psi initial pressure at room temperature of 10% H_2/Ar at 280 °C for 1 h. 20 mL 10 wt.% glycerol aqueous solution was the reactant. Catalyst weight was 50 mg of 3%Pt/C and 20 mg of 3%Pt-3%Re/C. The stirring rate was fixed at 600 rpm.

Catalyst	X_G (%)	Gas product composition (mol% dry basis)[a]				X_L (%)	Liquid product distribution (mol%)[b]								X_G/X_L
		H_2	CH_4	CO_2	C_{2^+}		LA	AA	EG	acetol	PG	MeOH	EtOH	PA	
3%Pt/C	6.2	65.4	1.3	30.4	3.8	6.7	14.4	2.7	13.3	15.1	45.3	1.2	6.9	1.1	0.9
3%Pt-3%Re/C	5.4	54.0	3.8	30.6	11.5	13.4	17.1	4.5	6.1	24.2	35.3	0.8	9.3	2.7	0.4

X_G, X_L: conversion to gas and liquid products, respectively; LA: lactic acid; AA: acetic acid; EG: ethylene glycol; PG: propylene glycol; PA: 1-propanol.

[a] Gas product is mainly composed of H_2, CH_4, CO and CO_2, C_2H_6 and C_3H_8. C_{2^+} includes C_2H_4, C_2H_6 and C_3H_8.
[b] Experimental data shown in this table was obtained at total carbon loss within 10%, most of which was caused by unknowns in liquid products.

Table 2 EXAFS fitting results for the Pt/C and Pt-Re/C catalysts at the Pt L_2 and Re L_3 edges. The catalysts were reduced at 300 °C in 100% H_2 and the EXAFS spectra were collected at 225 °C under 100% H_2 flow and atmospheric pressure or during APR at 500 psig and 225 °C.[a] The numbers in parentheses indicate the statistical error in the most significant digit obtained from the fit in Artemis (e.g., 6.2(8) ≡ 6.2±0.8).

Edge	Sample	Condition (at 225 °C)	Absorber-backscatterer pair	CN	R (Å)	σ^2 (Å^2)	ΔE_0 (eV)	Reduced χ^2
Pt L_2	Pt/C	H_2	Pt-Pt	8.5(9)	2.749(7)	0.012(1)	5.6(8)	25
		APR	Pt-Pt	10.4(1.3)	2.759(8)	0.012(1)	5.7(9)	49
	Pt-Re/C	H_2	Pt-M	7.0(8)	2.735(9)	0.009(1)	6.2(7)	86
		APR	Pt-M	9.1(1.1)	2.750(7)	0.010(1)	6.3(9)	43
Re L_3	Pt-Re/C	H_2	Re-M	6.2(8)	2.677(4)	0.013(1)	3.2(1.5)	29
			Re-O1	1.1(3)	1.74(1)	0.006(2)	1.0(1.5)	
			Re-O2	1.2(4)	2.00(1)	0.006(2)	1.0(1.5)	
		APR	Re-M	8.9(9)	2.716(6)	0.009(1)	5.3(1.0)	97
			Re-O1	0.9(2)	1.75(2)	0.007(2)	5.3(1.0)	
			Re-O2	2.6(5)	2.00(1)	0.007(2)	5.3(1.0)	

[a] No significant difference in the catalyst performance or structure (XAFS) was found by increasing the reduction temperature from 280 to 300 °C or by increasing the H_2 partial pressure from 10% to 100% (not shown).

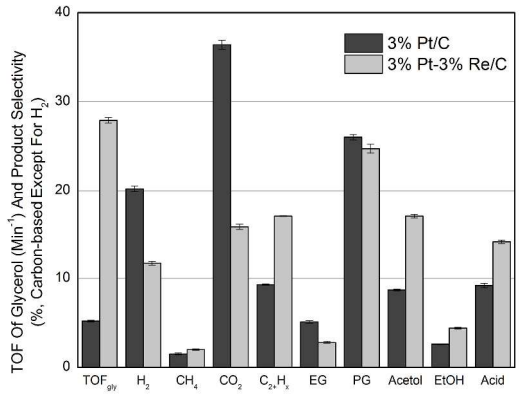

Figure 1. TOF of glycerol (min^{-1}) and product selectivity for APR of 20 mL 10 wt.% glycerol aqueous solution over 3%Pt/C and 3%Pt–3%Re/C at 225 °C. Loaded catalyst weight was 50 mg of 3%Pt/C and 20 mg of 3%Pt-3%Re/C to achieve similar conversion level (<20%). H_2 selectivity is defined as the ratio of H_2 produced to the maximum H_2 that could be produced from the converted glycerol. Selectivity to other carbon-containing products (in both gas and liquid phases) are normalized and calculated based on moles of carbon in the product

3.2. Catalyst properties in aqueous-phase environment

3.2.1 CO adsorption

We recently reported on the *in situ* ATR-IR characterizations of Pt/C and Pt-Re/C catalyst surfaces under reducing and steam environments, and found that CO desorption is significantly more facile on Pt-Re/C after steam treatment[12]. In this work, we further explored the utilization of this technique and extended its capability to *in situ* high pressure liquid environment, simulating APR reaction condition.

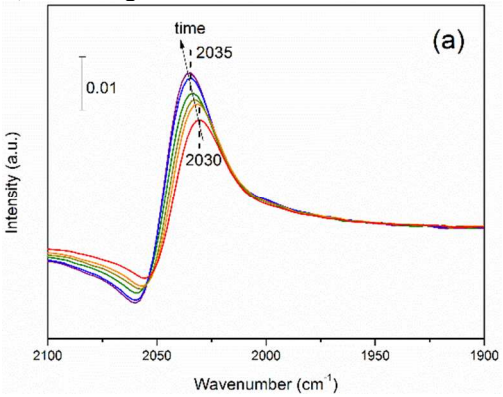

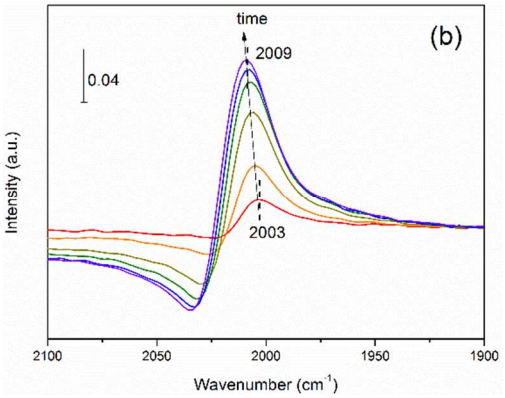

Figure 2. CO adsorption at room temperature (time interval = 1.5 min) on Pt/C under (a) gas and (b) aqueous phase

The spectra of CO adsorption on Pt/C under dry and high pressure water environments are compared in Figure 2 as an example. In Figure 2(a), linearly adsorbed CO on Pt^0 site was initially observed at 2030 cm^{-1}, which gradually shifted to 2035 cm^{-1} at saturation level due to dipole-dipole coupling caused by the increasing surface coverage[21]. In Figure 2(b), in the presence of high pressure water, linearly adsorbed CO on Pt^0 site was detected at 2004 cm^{-1} and gradually shifted to 2009 cm^{-1}, due to the same dipole-dipole coupling[21]. The slower profile development of CO adsorption spectrum in Figure 2(b) is because of a much lower CO concentration. The redshift of CO adsorption peak and about a factor of four spectrum intensity enhancement from gas to aqueous phase are consistent with observations by Ebbesen et al. and can be attributed to the direct effect of water on the transition dipole moment of the adsorbed CO[21]. Such redshift of CO adsorption and spectrum intensity enhancement from gas to aqueous phase were also observed at above room temperature of CO adsorption (Figure 3).

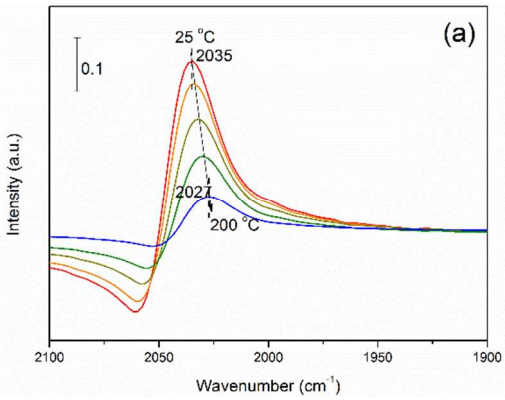

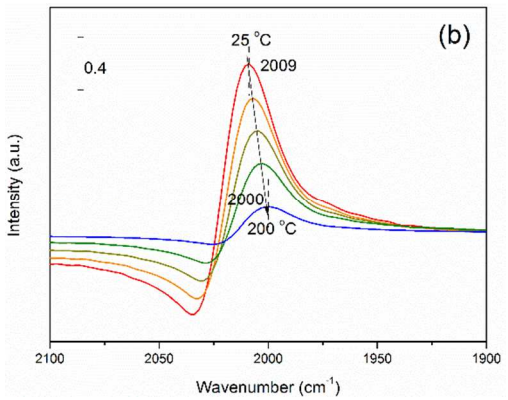

Figure 3. CO adsorption at different temperatures on Pt/C in (a) gas and (b) aqueous phase

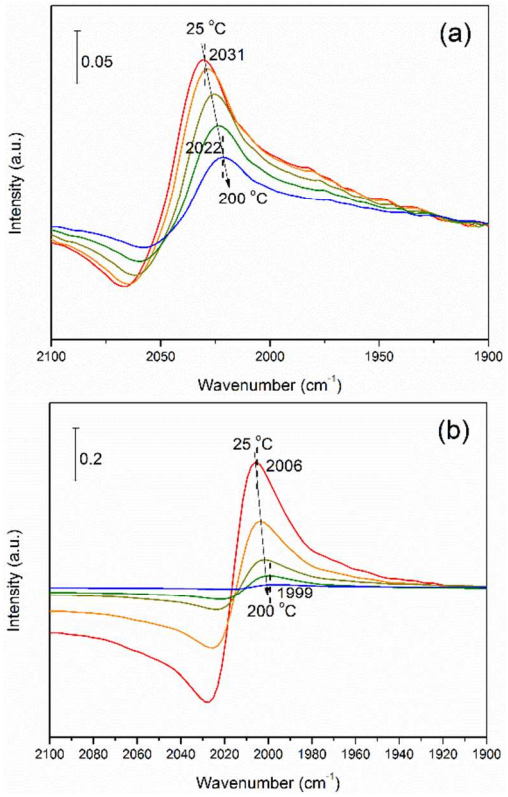

Figure 4. CO adsorption at different temperatures on Pt-Re/C in (a) gas and (b) aqueous phase

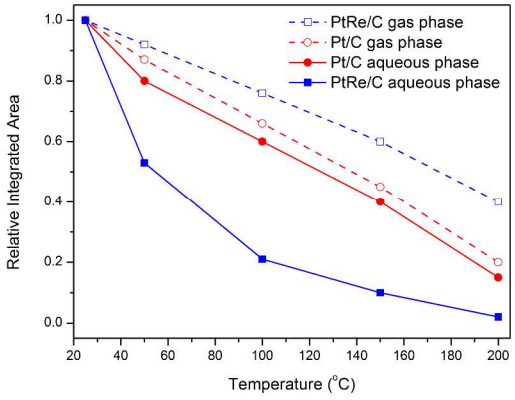

Figure 5. Relative integrated peak area as a function to desorption temperature of Pt/C and Pt-Re/C in gas or aqueous phase

As shown in Figures 4, a CO adsorption peak shift of 25 cm^{-1} was also observed on Pt-Re/C between gas and aqueous phase treatment, which is caused by the presence of condensed water[21]. The intensity of spectra over Pt-Re/C catalyst is about half that of Pt/C for both gas and aqueous phases (Figures 3 and 4), which is consistent with our previous report that Pt dispersion is decreased by half with the addition of Re to Pt/C[12]. CO adsorption on Pt/C and Pt-Re/C under gas or aqueous phase displayed different vibrational features and the adsorption peak maxima at 25 °C were centered at 2035, 2009, 2031, and 2006 cm^{-1} for Pt/C gas, Pt/C aqueous, Pt-Re/C gas, and Pt-Re/C aqueous respectively. These features can all be ascribed to linear CO adsorption (CO_L) on Pt site[22], while CO adsorbed on bridge or multi-fold sites was negligible. Upon TPD, the peak maxima red-shifted and the peak areas decreased. As shown in Figure 5, for Pt/C, the relative integrated peak area of CO adsorption in aqueous phase dropped by less than 10% at each temperature compared to its gas phase adsorption profile. However, for Pt-Re/C the amount of CO adsorption in aqueous phase decreased by about half at 50 °C and almost dropped to zero around 180-200 °C. The comparison of CO TPD in the gas phase shows that CO is more strongly adsorbed on PtRe than on Pt. On the other hand, under aqueous phase conditions the results are analogous to our previous observation on steam-treated samples where the CO desorption from catalyst surface was more facile on PtRe compared to Pt/C.

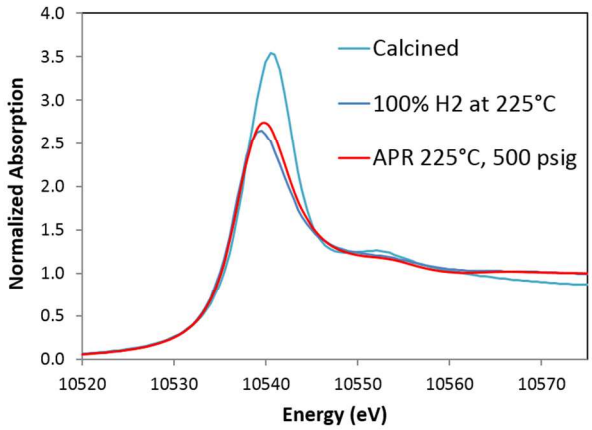

Figure 6. XAFS spectra of Re L_3 edge under APR and reduction conditions

We previously reported the investigation of the electronic and structural properties of the catalysts by XANES and EXAFS under different gas environments[12]. We showed that the formation of Pt-Re alloy results in an insignificant charge transfer between Pt and Re. From the XANES spectra, we showed that the alloy formation results in a possible narrowing of the Pt d-DOS, likely as a result of the hybridization between the Pt and Re d-bands. Moreover, since there is minimal charge transfer between Pt and Re, a narrowing of the d-DOS should be expected to result in the upward shift of the d-band center relative to the Fermi level according to the "rectangular band" model[23]. The conclusions from XAFS were consistent with the stronger CO adsorption as shown by CO ATR-

IR and TPD[12]. To determine the effect of APR reaction conditions on the catalyst structural and electronic properties, in-operando XAFS of Pt/C and Pt-Re/C catalysts was performed and compared to that under reducing environment. The EXAFS fitting for both catalysts are listed in Table 2. It can be seen that the APR conditions result in an increase in the Pt-M and Re-M coordination numbers which is consistent with an increase in particle size during APR as we reported previously by *ex situ* TEM[10]. Additionally, the Re-O coordination increased despite the increase in particle size which suggests that the percentage of ReOx on the surface was significantly higher during APR than after reduction. Figure 6 shows the XANES spectra at the Re L_3 edge under reducing conditions and during APR. Clearly, it can be seen that the Re L_3 edge shifts to higher energy and the white line intensity increases, which is consistent with the partial oxidation of Re and/or adsorption of OH on Re[12] which is consistent with the higher ReO_x percentage concluded from EXAFS. The oxidation of Re was investigated further by Raman spectroscopy as discussed below. The small differences between the Pt $L_{2,3}$ XANES spectra of Pt and PtRe during APR (see SI) can be mostly attributed to difference in the coverage of adsorbates. No Pt oxidation was detected by XANES or EXAFS for either catalyst, Pt/C or PtRe/C, consistent with previous reports on Pt and PtMo[3].

3.2.2 Raman study of Pt-Re/C catalyst and Re leaching

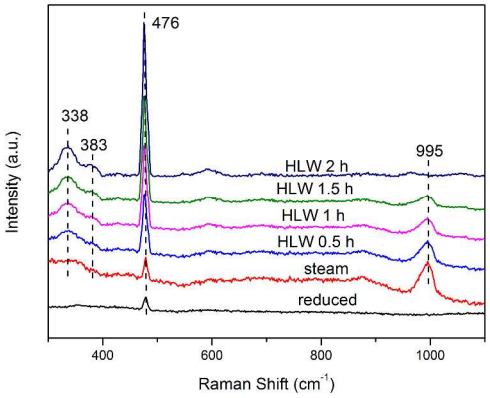

Figure 7. Raman spectra of Pt-Re/C catalyst after reduction, steam or hot liquid water (HLW, for 0.5, 1, 1.5, and 2 h) treatment

In order to understand the impact of water treatment on the catalyst surface structure, Raman study of Pt-Re/C catalyst was carried out. Figure 7 depicts the Raman spectra of Pt-Re/C catalyst after reduction, steam or HLW, respectively. The reduced sample shows only one small peak at 478 cm^{-1}, while after steam treatment a peak at 995 cm^{-1} shows up as previously reported[12]. Introduction of steam following reduction had a negligible effect on the feature at 478 cm^{-1} but gave rise to the band at 995 cm^{-1}. Literature has reported[24] that the latter could be assigned to terminal Re-O symmetric stretching from tetrahedrally coordinated ReO_4 unit[25] on the catalyst surface. Upon HLW treatment, the 478 cm^{-1} peak increases, whereas the 995 cm^{-1} peak decreases as a function of time. The sample with 2 h HLW treatment exhibits four Raman bands (338, 383, 478, and 594 cm^{-1}) with the 478 cm^{-1} band being most prominent. More specifically, the 478 cm^{-1} feature has been assigned to the M-O-Re symmetric stretching mode with low-valent Re species or low coordination ReO_x cluster[12]. Because the existence of Pt-O-Re linkage is not supported by our XANES characterization at the Pt L_3 edge (Figure S1), assigning this feature to Re-O-Re linkage is more likely. The low frequency band at 338 cm^{-1} along with a shoulder at 383 cm^{-1} was assigned to the degeneracy of the Re-O-Re bending modes. Although the bands here were observed at higher frequencies than previously reported, the band structure is consistent[24, 25]; the shift is likely due to the close association with Pt center. The Raman feature at 478 cm^{-1} was at the same frequency as that observed on both the reduced and steam-treated samples. This feature cannot be simply correlated with oxygen bonding between either Pt or Re as the closest possible Re features is at ~478 cm^{-1} for Re-O-Re symmetric stretching (very weak)[25] or the closest possible Pt feature at ~514 cm^{-1} for the A_{1g} symmetric breathing mode of α-PtO_2[26]. In order to properly assign this feature, the steam-treated catalyst was subjected to HLW treatment with the aim to leach out excess ReO_x not in contact/alloyed with Pt[10]. As shown in Figure 7, as exposure to HLW was extended, the terminal Re-O feature decreased, whereas the feature 478 cm^{-1} continued growing along with slight increase in the Re-O-Re bending mode intensity. As a result, it appears that the terminal Re-O is most vulnerable to leaching treatment, which is consistent with the fact that O-terminated Re_2O_7 readily dissolves in water via hydrolysis. Our previous report showed that although the Re content on the catalyst decreases by half after a week of APR reaction, the time-on-stream activity only drops by 10% with little change in selectivity[10]. In contrast, Re-O-Re increased slightly, this could be due to better dispersion or more oxidation of Re. This feature is also present on reduced and steam-treated sample. However, the intensity is relatively low, possibly due to the coverage by terminal Re-O. The Pt-Re/C catalyst surface structural changes after steam and HLW exposures are depicted in Scheme 1.

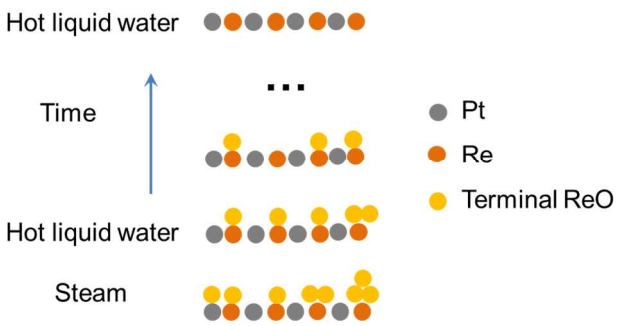

Scheme 1. Surface structural changes of Pt-Re/C after steam and HLW exposures

Following HLW treatment for up to 4 h, the samples were tested for APR reaction to understand how the surface properties of catalyst impact the activity. Glycerol was injected into the aqueous phase without exposing catalyst to air after the HLW treatment. Figure S2 shows the comparison of glycerol conversion over catalysts treated under HLW for 0.5, 1, 1.5, 2, and 4 h (product selectivity was the same as observed over samples not treated with HLW for both Pt/C and Pt-Re/C). Consistent with our prior report using a fixed bed reactor[10], Pt-Re/C activity appears to be less affected by this pretreatment, despite the leaching of Re occurring as evidenced by Raman spectroscopy and the result in Figure S3 showing the

actual amount of Re that is leached out. Therefore, the leached Re species from the catalyst surface must have a negligible impact on catalyst activity. Additionally, because of the very low amount of leached Re species in the aqueous phase, it is very unlikely that the dissolved Re species are participating as a homogenous catalyst.

3.2.3 Pyridine adsorption

In addition to surface acidity from the catalyst support, extra surface acidity derived from metallic sites (oxide/hydroxide) has been proposed to have a significant impact on the catalytic behavior[8, 10, 27]. Due to the strong absorption of infrared energy by carbon, conventional DRIFTS studies of the catalysts were only possible on Pt and PtRe on other non-carbon based supports, e.g. SiO_2 [10]. Thus, ATR-IR was here employed to monitor the surface acidic properties of Pt/C and Pt-Re/C catalysts with *in situ* treatments. In Figure 8, the characteristic features of different acid centers can be resolved and identified with the peak assignment allowing for differentiation among Brønsted sites (~1640 and 1540 cm^{-1}) and Lewis sites (~1610 and 1440 cm^{-1}).

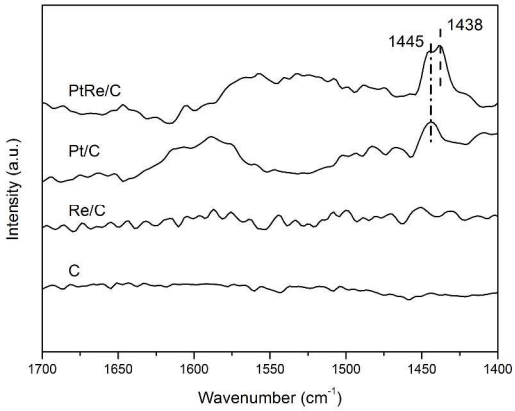

Figure 8. Pyridine adsorption on samples after HLW treatment characterized by ATR-IRS

As can be seen in Figure 8, carbon support and Re/C exhibit merely background signal. Although some organic groups, including phenolic and carboxylic, could be present on active carbon surface the concentration was too low to be detected and their contribution to the overall surface acidity is negligible. Zawadzki reported pyridine adsorption on carbon film and concluded that without substantially oxidizing the carbon film only physisorbed pyridine was present[28]. This is consistent with what was observed on the carbon support even after HLW treatment and also implies that the carbon support used in this study is stable (resistant to oxidation) under HLW treatment. The fact that there was no measureable acidity over the Re/C sample could be due to limited Re dispersion, coordination saturation of Re, and little OH on terminal ReO species[27]. Pt/C showed a broad feature centered at 1588 cm^{-1} with a shoulder at 1611 cm^{-1} which can be assigned to physically and coordinately adsorbed pyridine on Lewis acid sites, respectively. A less resolved weak peak with a center at 1482 cm^{-1} indicated the presence of either Brønsted or Lewis acidity as they can independently contribute to this feature. Because there was no Brønsted feature observed around 1540 cm^{-1}, it appears that only Lewis acidity exists. This was further confirmed by the clear band at 1445 cm^{-1} which is characteristic of Lewis acidity. These data suggest that after HLW treatment the Pt nanoparticle surface becomes electron deficient (likely due to adsorption of hydroxyl groups[10, 29]) and the exposed $Pt^{\delta+}$ acts as Lewis acid (LPy) for the coordination with pyridine molecule. After adding Re, it was observed that a broad peak (about 50 cm^{-1} wide) appears at ~1535 cm^{-1}, indicating C-N ring vibration of pyridium cation (PyH^+) adsorbed on Brønsted acid sites of catalyst surface (Pt/C does not show this feature). An additional feature appeared at 1635 cm^{-1}, confirming the presence of Brønsted acidity. At least three sets of experiment were carried out to make sure the peaks observed here are not due to spectrum noise. In addition to the peak at 1445 cm^{-1}, another feature of Lewis acidity appeared at 1438 cm^{-1}, forming a doublet. This new feature could arise from pyridine molecule coordinately adsorbed on exposed $Re^{\delta+}$. The difference in wavenumber (7 cm^{-1}) indicates that Lewis acidity associated with Re is stronger than that with Pt. Moreover, by deconvolution and comparison of the peak area for 1445 and 1438 cm^{-1}, the amount of Lewis acidity associated with Pt and Re, respectively, appeared to be very similar. This is consistent with the chemisorption measurement showing that after adding Re, the Pt dispersion decreased by about half.

3.3 Role of Re species in APR

The primary function of Re species observed in this work is to enhance the activity of Pt/C catalyst. This enhancement has previously been related to the weakened interaction between CO and Pt surface modified by Re. However, our *in situ* ATR-IRS study on reduced catalyst does not support this hypothesis. We previously reported that after steam exposure at steam reforming temperature, CO desorption became more facile from Pt-Re/C than that from Pt/C[12]. Here we employed the same *in situ* ATR-IRS technique under simulated APR condition to investigate CO adsorption behavior in condensed water environment. The results over Pt/C and Pt-Re/C catalysts are shown in Figure 5. Pt/C shows only linear CO desorption, and about 20% of the peak area is retained at 200 °C. Facile CO desorption occurs at low temperatures over Pt-Re/C, and less than 20% peak area remains at 100 °C. Considering the difference of the catalyst surface, it is possible that, due to its oxophilicity nature, ReO_x may facilitate CO transfer from neighboring Pt site via interacting with the O atom, leading to facile CO desorption. This is consistent with our observation for steam-treated catalysts. The overall activity enhancement over Pt-Re/C catalyst in aqueous-phase reforming is also in good agreement with our previous conclusion in glycerol steam reforming. Since in condensed water the close proximity between Pt and oxidized Re on Pt-Re/C catalyst surface is not affected and is comparable to that after steam treatment, CO spillover from Pt site to the neighboring Re oxide species that we previously reported[12] could be used to explain the observed activity enhancement. Moreover, the leached Re oxide species do not seem to contribute to this enhancement.

The preferable reaction pathway of glycerol reforming to produce hydrogen should consist of primarily dehydrogenation and decarbonylation. It is generally accepted that Pt surface can catalyze dehydrogenation[30] and a small portion of dehydration[31] of glycerol. Questions remain about how the addition of a second metal affects the overall catalytic activities of the catalyst and whether the reaction environment has any effect. In contrast to the statement by Lin[30] that doping

Re acts as a basic promoter like KOH, under the hydrothermal condition Re is believed to present as oxide/hydroxide/hydrate species providing (additional) acid site[8, 10, 27], or to coordinate with Pt presenting different types of acid site as evidenced in this paper. As previously reported, Re in non-zero oxidation states (e.g., ReO_x) could provide sites for CO oxidation[32] and water activation[33]. In Figure 1, Pt-Re/C catalyst shows much lower H_2 and CO_2 selectivities compared to Pt/C catalyst. This has been well correlated to the C-C and C-O bond cleavage ability as we recently reported[10]. The preferred pathway (all the way including water-gas shift) in glycerol APR should produce H_2 and CO_2 according to equation $C_3H_8O_3+3H_2O \rightarrow 7H_2+3CO_2$. However, the decrease in CO_2 selectivity is more pronounced over Pt-Re/C as shown in Figure 1. Besides, acetol selectivity over Pt-Re/C is almost doubled, whereas propylene glycol selectivity remains about the same. Therefore, it can be suggested that the reaction pathway is significantly shifted from dehydrogenation over Pt/C to dehydration over Pt-Re/C, while hydrogenation of the dehydrated product is also less favored over Pt-Re/C. The lower ethylene glycol production and higher selectivity of ethanol and C_{2+} alkanes also support the more favored dehydration pathway.

It has been evidenced by both CO chemisorption and pyridine adsorption measurement that compared with 3%Pt/C, Pt dispersion is decreased by about half on 3%Pt-3%Re/C. It is possible that well-mixed bimetallic surface enhances the catalytic turnover and results in the observed higher TOF over Pt-Re/C catalyst. On such bimetallic surface, Pt acts as the adsorption and main reaction site for dehydrogenation and C-C cleavage, while Re provides the site for temporal accommodation of CO molecule and its desorption or water-gas shift. A possible reaction route is shown in Scheme 2. Scheme 2(b) shows the APR reaction route of which the decomposition product CO could be transferred from metallic Pt to the neighboring Re site through the higher affinity of oxygen atom to Re. In aqueous phase reforming, the terminal Re-O structure may only serve as spectator which also leaches out under hot liquid water condition as evidenced by Raman (Figure 7), while the active structure for APR reaction involves both Pt and Re governing the activity and selectivity despite the inactive Re species leaching into the solution. The APR active structure consists of coordinately unsaturated Pt and Re atoms due to the reaction environment, as evidenced the Raman and pyridine ATR-IR (Figure 8). Acidity brought by these species facilitates the production of acetol as the major dehydration intermediate[34]. Pyridine ATR-IR showed that coordinatively unsaturated Pt and Re atoms on the catalyst surface could provide Lewis acidity, and their amounts are comparable based on the result of 3%Pt-3%Re/C catalyst shown in Figure 8. The selectivity of acetol, dehydration product of glycerol catalyzed by Lewis acid site[35], over Pt-Re/C catalyst is about doubled compared to that over Pt/C. Therefore, the amount of Lewis acidity agrees well with the initial step of glycerol dehydration via Lewis acid site. Although Brønsted acidity is also present as characterized by pyridine adsorption by ATR-IRS in Figure 8, its participation in the initial dehydration step is negligible because of the absence of propanal and acrolein (via dehydration) or 1,3-propandiol (via hydrogenolysis), which are generally accepted as glycerol dehydration product via proton-catalyzed pathway[36, 37]. However, such Brønsted acidity could participate in the hydrogenolysis pathway along with Pt site[35]. Scheme 2 shows the reaction route of glycerol aqueous-phase reforming and the possible pathway on each site. Glycerol decomposition is initiated via adsorption on Pt site. Exposed coordinatively unsaturated Pt and Re atoms under reaction condition can serve as Lewis acid sites, which are responsible for the dehydration pathway, competing with the C-C cleavage and thus suppress the formation of hydrogen and CO_2. The synergy between Pt sites and Brønsted acid sites contribute to the hydrogenolysis reaction pathway.

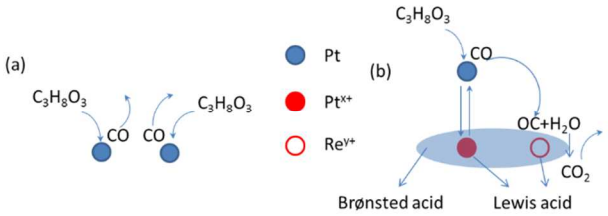

Scheme 2. APR of glycerol over (a) Pt/C and (b) Pt-Re/C catalysts

4. Conclusions

Bimetallic Pt-Re/C catalyst showed enhanced catalytic activity compared to monometallic Pt/C catalyst in glycerol APR. Similar to glycerol steam reforming, the enhancement of activity was found to be due to more facile CO desorption from Pt-Re/C than that from Pt/C under simulated APR condition. Contrary to glycerol steam reforming, liquid product is more favored over Pt-Re/C at the expense of H_2 and CO_2 selectivity in glycerol APR compared to that on Pt/C. This could be due to the extent of Re oxidation under APR reaction condition since XANES shows that, compared to steam treatment, APR reaction environment further oxidizes the surface Re species. Raman characterization of Pt-Re/C catalyst after HLW treatment, simulating APR environment, indicated the presence of both well-dispersed Re oxide species (characterized by the Re-O-Re linkage) associated with Pt sites and Re oxide species with terminal Re-O. However, the Re oxide species with terminal Re-O can be readily leached out under APR conditions and have little influence on the product selectivity in glycerol APR. The leaching of Re oxide species with terminal Re-O in glycerol APR likely exposes the well-dispersed Re oxide species associated with Pt sites, which is selective towards liquid product formation. Such structure with coordinately unsaturated Pt and Re atoms could act as Lewis acid sites catalyzing the initial dehydration of glycerol to hydroxyacetone (acetol), leading to completely different product selectivity in glycerol APR on Pt-Re/C compared to that on Pt/C. Brønsted acidity is also present on Pt-Re/C, which could originate from the bridging hydroxyl in the M-OH-M moiety. However, Brønsted acidity does not seem to compete with Lewis acidity in the initial dehydration step in glycerol APR due to the absence of Brønsted acid catalyzed product formation.

AUTHOR INFORMATION

Corresponding Author

* Y. W.: Phone: +1 (509) 371-6273. Fax: +1 (509) 371-6242. E-mail: yong.wang@pnnl.gov.
* A.M.K: phone: 540-231-9138, E-mail: amkarim@vt.edu

Present Addresses

† Present address: Johnson Matthey Inc., 900 Forge Avenue, Suite 100, Audubon, PA 19403, USA

‡ Present address: Department of Chemical Engineering, Virginia Polytechnic Institute and State University, Blacksburg, Virginia 24061, USA

Author Contributions

The manuscript was written through contributions of all authors. All authors have given approval to the final version of the manuscript.

ACKNOWLEDGMENT

The authors acknowledge financial support from US Department of Energy (DOE), Office of Basic Energy Sciences, Division of Chemical Sciences, Geosciences, and Biosciences. Use of the National Synchrotron Light Source, Brookhaven National Laboratory, for the EXAFS experiments was supported by the US Department of Energy, Office of Basic Energy Sciences (Grant# DE-FG02-05ER15688). Beam line X18A is supported, in part, by the Synchrotron Catalysis Consortium. A.M.K. would like to thank Yongchun Hong (Washington State University) for his help with the XAS data collection.

Supporting Information Available

Effect of hot liquid water (HLW) treatment duration on glycerol conversion in APR and the percentage of Re retained on the Pt-Re/C catalyst and leached into the liquid phase. EXAFS and XANES spectra under APR and reducing environments. This material is available free of charge via the Internet at http://pubs.acs.org/.

REFERENCES

[1] Cortright, R.D., Davda, R.R., Dumesic, J.A., *Nature*, **2002**, 418. 964-967.
[2] Wen, G., Xu, Y., Ma, H., Xu, Z., Tian, Z., *Int. J. Hydrogen Energy*, **2008**, 33. 6657-6666.
[3] Dietrich, P., Lobo-Lapidus, R., Wu, T., Sumer, A., Akatay, M., Fingland, B., Guo, N., Dumesic, J., Marshall, C., Stach, E., Jellinek, J., Delgass, W., Ribeiro, F., Miller, J., *Top. Catal.*, **2012**, 55. 53-69.
[4] Dietrich, P., Wu, T., Sumer, A., Dumesic, J., Jellinek, J., Delgass, W.N., Ribeiro, F., Miller, J., *Top. Catal.*, **2013**, 56. 1814-1828.
[5] Tupy, S.A., Karim, A.M., Bagia, C., Deng, W., Huang, Y., Vlachos, D.G., Chen, J.G., *ACS Catal.*, **2012**, 2. 2290-2296.
[6] Yu, W., Porosoff, M.D., Chen, J.G., *Chem. Rev.*, **2012**, 112. 5780-5817.
[7] Kunkes, E.L., Simonetti, D.A., Dumesic, J.A., Pyrz, W.D., Murillo, L.E., Chen, J.G.G., Buttrey, D.J., *J. Catal.*, **2008**, 260. 164-177.
[8] King, D.L., Zhang, L.A., Xia, G., Karim, A.M., Heldebrant, D.J., Wang, X.Q., Peterson, T., Wang, Y., *Appl. Catal., B*, **2010**, 99. 206-213.
[9] Wei, Z., Sun, J., Li, Y., Datye, A.K., Wang, Y., *Chem. Soc. Rev.*, **2012**, 41. 7994-8008.
[10] Zhang, L., Karim, A.M., Engelhard, M.H., Wei, Z.H., King, D.L., Wang, Y., *J. Catal.*, **2012**, 287. 37-43.
[11] Ciftci, A., Ligthart, D.A.J.M., Sen, A.O., van Hoof, A.J.F., Friedrich, H., Hensen, E.J.M., *J. Catal.*, **2014**, 311. 88-101.
[12] Wei, Z., Karim, A.M., Li, Y., King, D.L., Wang, Y., *J. Catal.*, **2015**, 322. 49-59.
[13] Ebbesen, S.D., Mojet, B.L., Lefferts, L., *Langmuir*, **2005**, 22. 1079-1085.
[14] Li, Y., Wei, Z., Sun, J., Gao, F., Peden, C.H.F., Wang, Y., *J. Phys. Chem. C*, **2013**, 117. 5722-5729.
[15] Karim, A.M., Howard, C., Roberts, B., Kovarik, L., Zhang, L., King, D.L., Wang, Y., *ACS Catal.*, **2012**, 2. 2387-2394.
[16] Newville, M., *J. Synchrotron Radiat.*, **2001**, 8. 96-100.
[17] Ravel, B., Newville, M., *J. Synchrotron Radiat.*, **2005**, 12. 537-541.
[18] Bare, S.R., Kelly, S.D., D.Vila, F., Boldingh, E., Karapetrova, E., Kas, J., Mickelson, G.E., Modica, F.S., Yang, N., Rehr, J.J., *J. Phys. Chem. C*, **2011**, 115. 5740-5755.
[19] Roldan Cuenya, B., Croy, J.R., Mostafa, S., Behafarid, F., Li, L., Zhang, Z., Yang, J.C., Wang, Q., Frenkel, A.I., *J. Am. Chem. Soc.*, **2010**, 132. 8747-8756.
[20] Kirilin, A.V., Hasse, B., Tokarev, A.V., Kustov, L.M., Baeva, G.N., Bragina, G.O., Stakheev, A.Y., Rautio, A.-R., Salmi, T., Etzold, B.J.M., Mikkola, J.-P., Murzin, D.Y., *Catal. Sci. Technol.*, **2014**, 4. 387-401.
[21] Ebbesen, S.D., Mojet, B.L., Lefferts, L., *J. Catal.*, **2007**, 246. 66-73.
[22] Mojet, B.L., Ebbesen, S.D., Lefferts, L., *Chem. Soc. Rev.*, **2010**, 39. 4643-4655.
[23] Schweitzer, N., Xin, H., Nikolla, E., Miller, J., Linic, S., *Top. Catal.*, **2010**, 53. 348-356.
[24] Williams, K.P.J., Harrison, K., *J. Chem. Soc., Faraday Trans.*, **1990**, 86. 1603-1606.
[25] Hardcastle, F.D., Wachs, I.E., Horsley, J.A., Via, G.H., *J. Mol. Catal.*, **1988**, 46. 15-36.
[26] McBride, J.R., Graham, G.W., Peters, C.R., Weber, W.H., *J. Appl. Phys.*, **1991**, 69. 1596-1604.
[27] Chia, M., Pagan-Torres, Y.J., Hibbitts, D., Tan, Q.H., Pham, H.N., Datye, A.K., Neurock, M., Davis, R.J., Dumesic, J.A., *J. Am. Chem. Soc.*, **2011**, 133. 12675-12689.
[28] Zawadzki, J., *Carbon*, **1988**, 26. 627-633.
[29] Yakovlev, A.L., Neyman, K.M., Zhidomirov, G.M., Rösch, N., *J. Phys. Chem.*, **1996**, 100. 3482-3487.
[30] Lin, Y.-C., *Int. J. Hydrogen Energy*, **2013**, 38. 2678-2700.
[31] Wawrzetz, A., Peng, B., Hrabar, A., Jentys, A., Lemonidou, A.A., Lercher, J.A., *J. Catal.*, **2010**, 269. 411-420.
[32] Ishida, Y., Ebashi, T., Ito, S.-i., Kubota, T., Kunimori, K., Tomishige, K., *Chem. Commun.*, **2009**, 5308-5310.
[33] Azzam, K.G., Babich, I.V., Seshan, K., Mojet, B.L., Lefferts, L., *ChemCatChem*, **2013**, 5. 557-564.
[34] Katryniok, B., Paul, S., Belliere-Baca, V., Rey, P., Dumeignil, F., *Green Chem.*, **2010**, 12. 2079-2098.
[35] Katryniok, B., Paul, S., Dumeignil, F., *ACS Catal.*, **2013**, 3. 1819-1834.
[36] ten Dam, J., Hanefeld, U., *ChemSusChem*, **2011**, 4. 1017-1034.
[37] Foo, G.S., Wei, D., Sholl, D.S., Sievers, C., *ACS Catal.*, **2014**, 4. 3180-3192.

Table of Contents

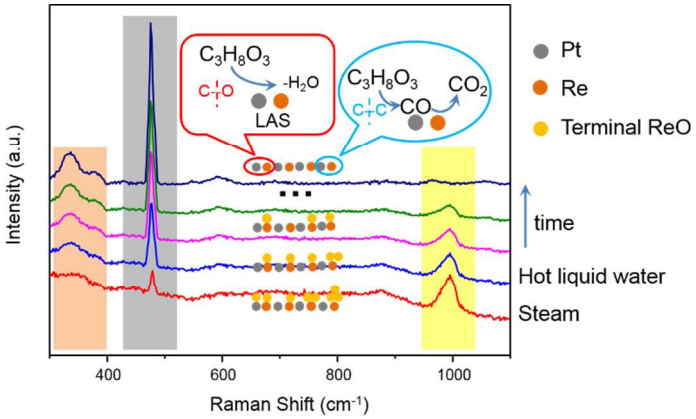

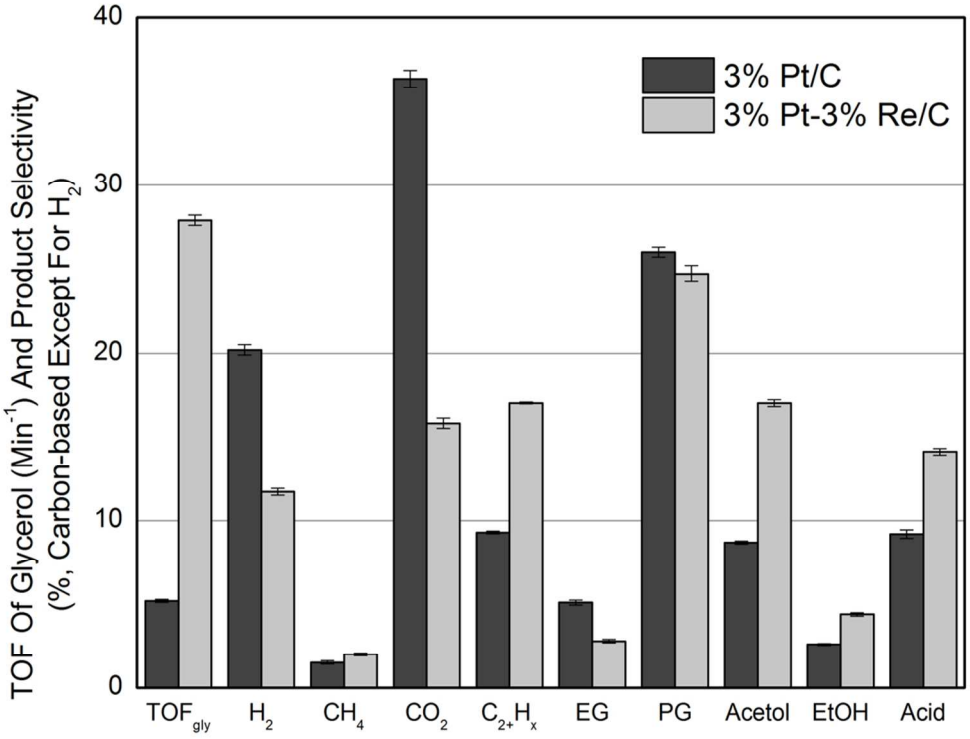

Figure 1. TOF of glycerol (min^{-1}) and product selectivity for APR of 20 mL 10 wt.% glycerol aqueous solution over 3%Pt/C and 3%Pt–3%Re/C at 225 °C. Loaded catalyst weight was 50 mg of 3%Pt/C and 20 mg of 3%Pt-3%Re/C to achieve similar conversion level (<20%). H_2 selectivity is defined as the ratio of H_2 produced to the maximum H_2 that could be produced from the converted glycerol. Selectivity to other carbon-containing products (in both gas and liquid phases) are normalized and calculated based on moles of carbon in the product
204x153mm (150 x 150 DPI)

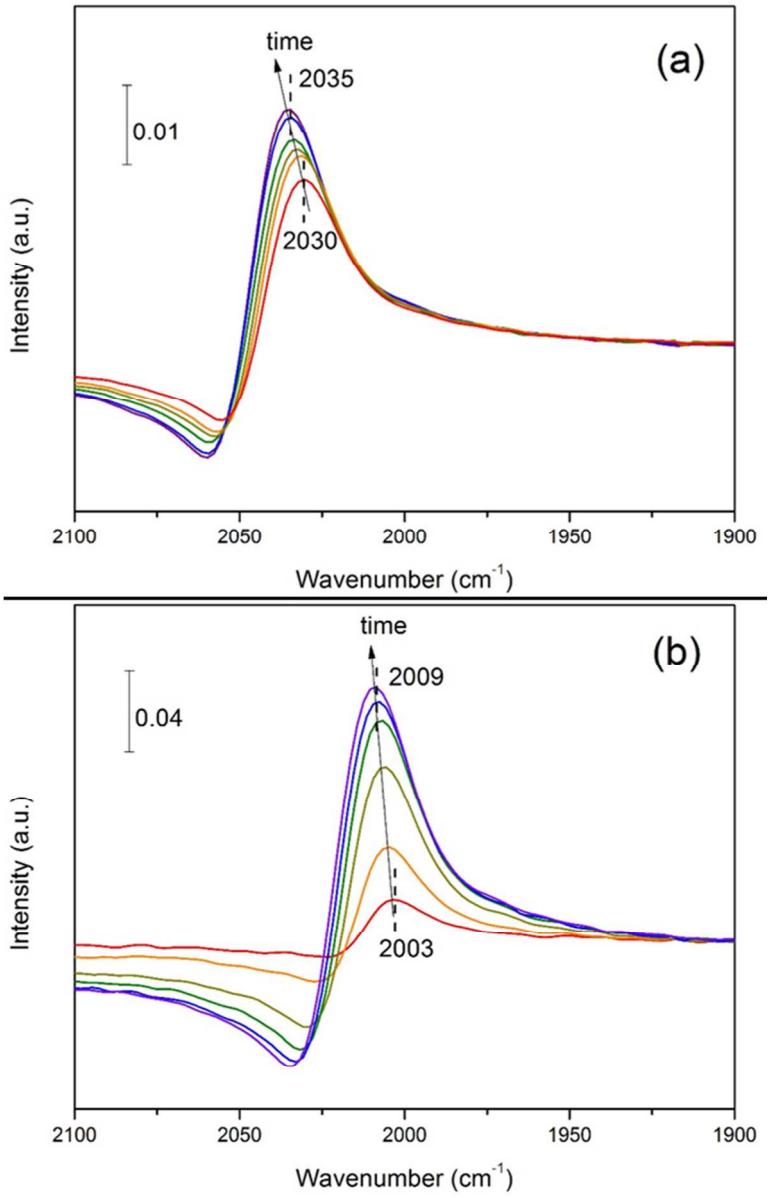

Figure 2. CO adsorption at room temperature (time interval = 1.5 min) on Pt/C under (a) gas and (b) aqueous phase
119x188mm (150 x 150 DPI)

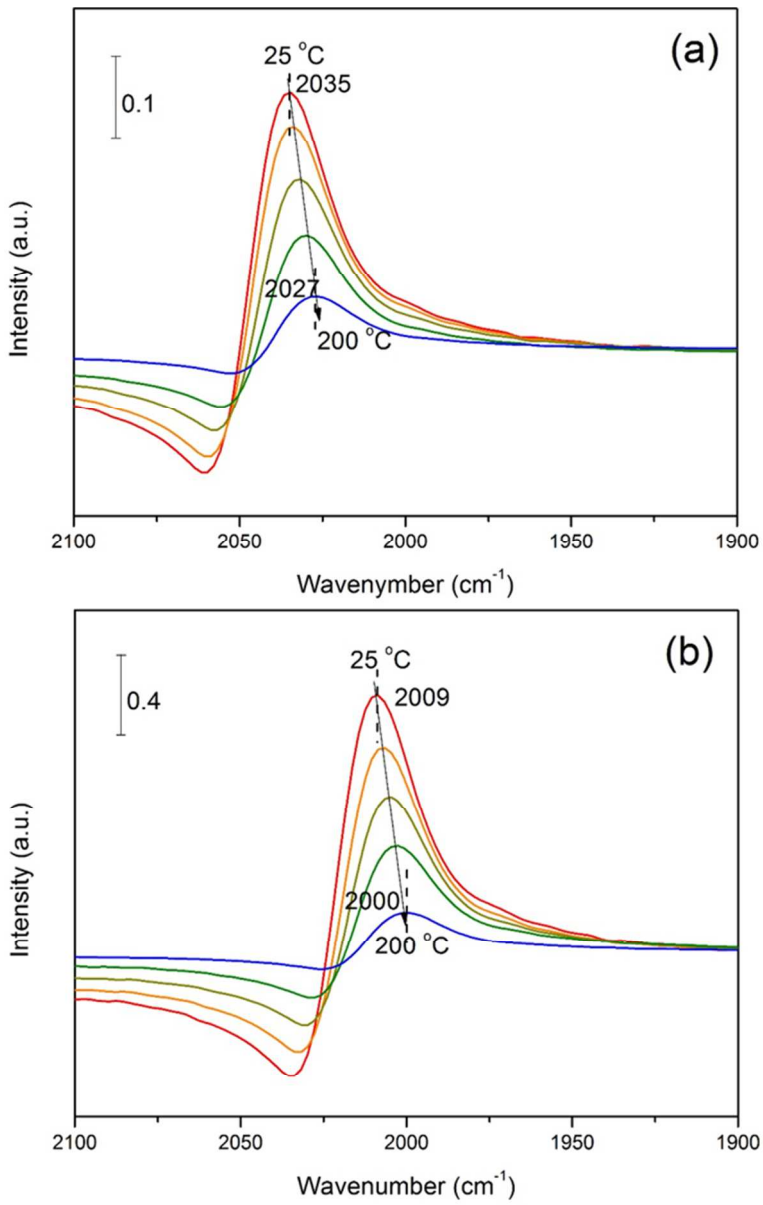

Figure 3. CO adsorption at different temperatures on Pt/C in (a) gas and (b) aqueous phase
125x196mm (150 x 150 DPI)

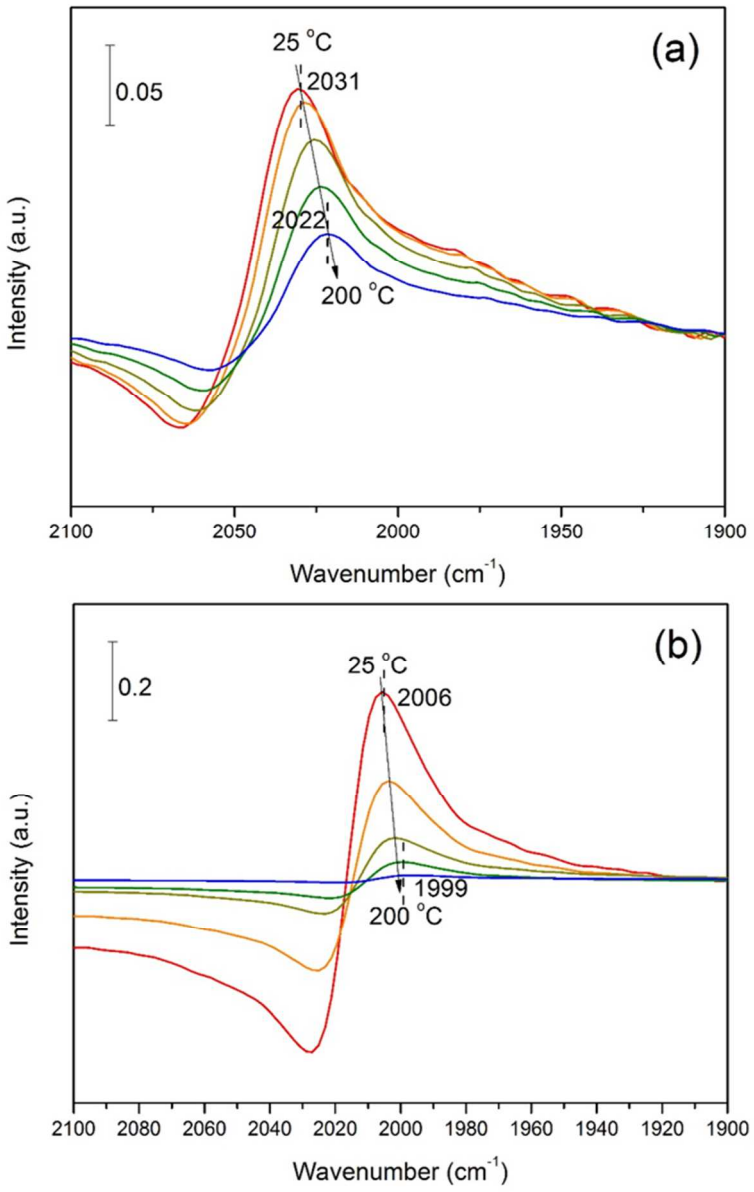

Figure 4. CO adsorption at different temperatures on Pt-Re/C in (a) gas and (b) aqueous phase
114x178mm (150 x 150 DPI)

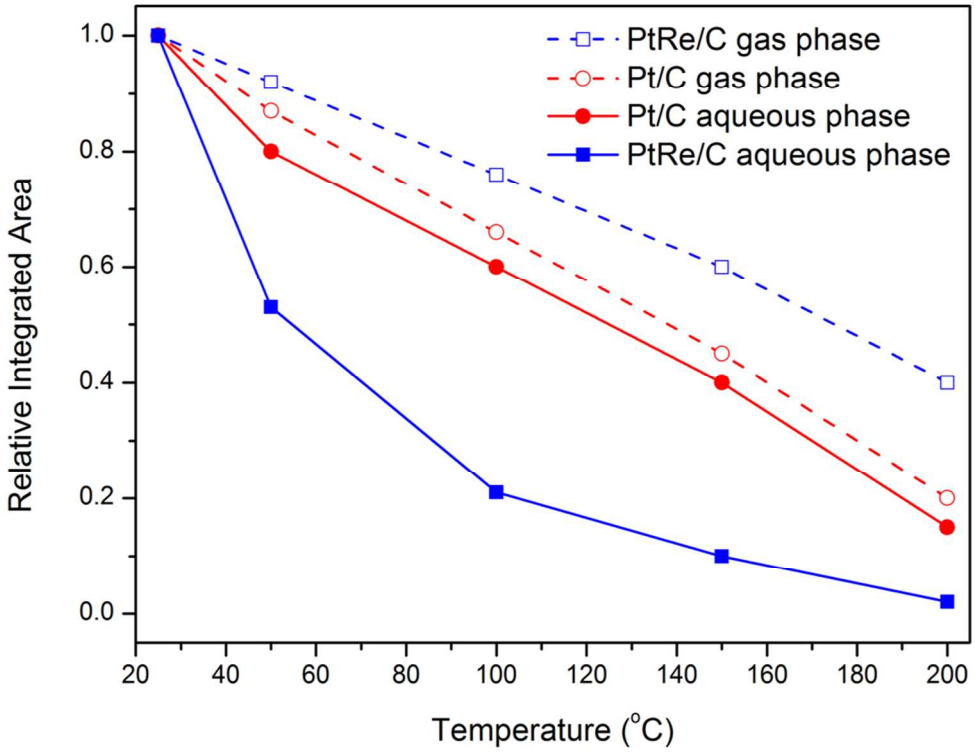

Figure 5. Relative integrated peak area as a function to desorption temperature of Pt/C and Pt-Re/C in gas or aqueous phase
207x160mm (150 x 150 DPI)

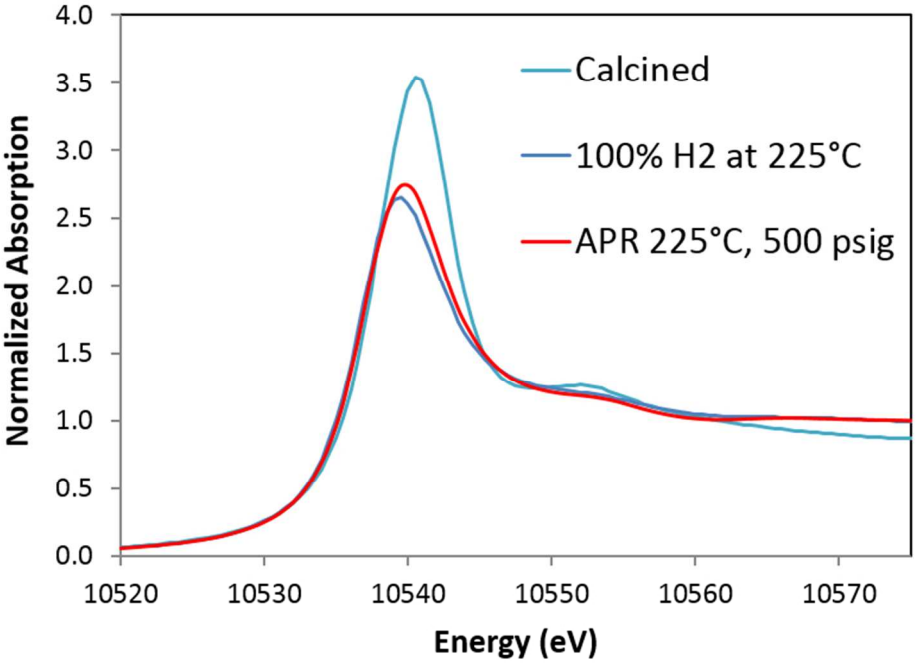

Figure 6. XAFS spectra of Re L_3 edge under APR and reduction conditions
142x100mm (150 x 150 DPI)

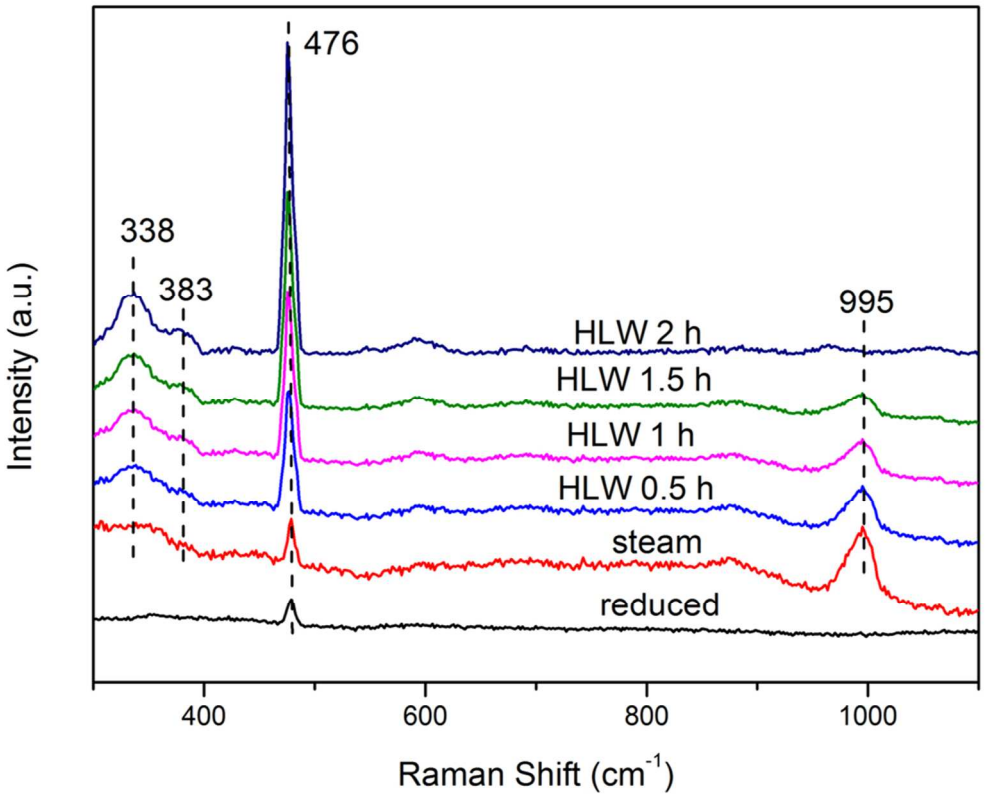

196x160mm (150 x 150 DPI)

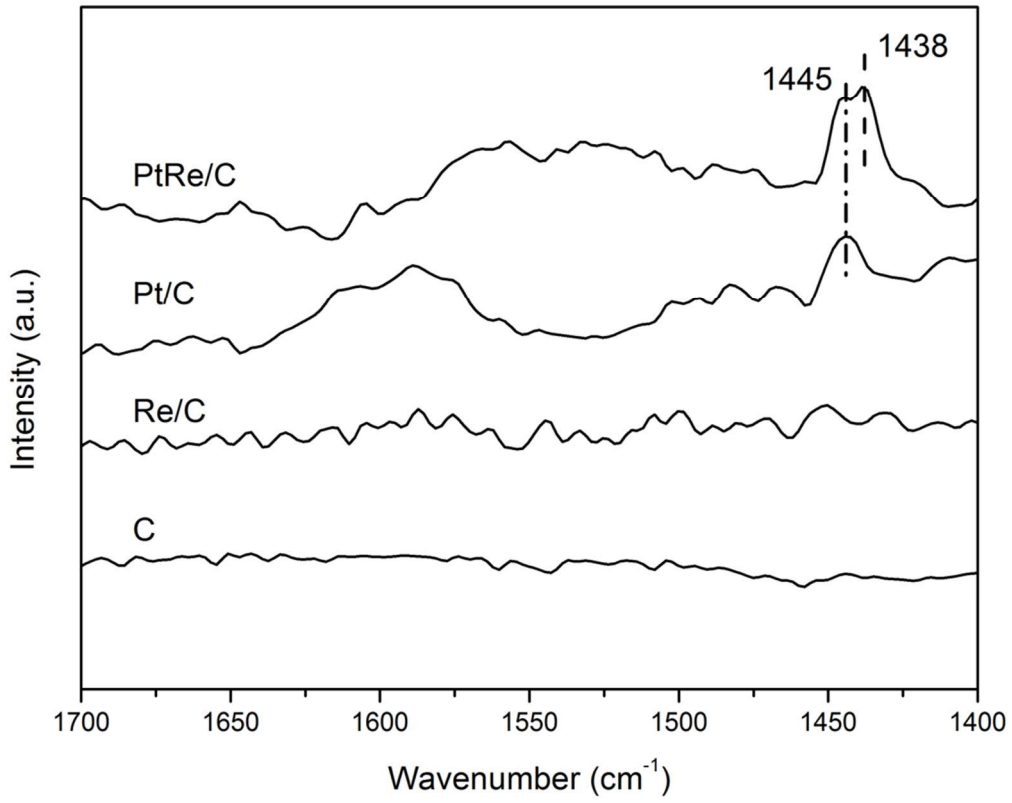

202x162mm (150 x 150 DPI)

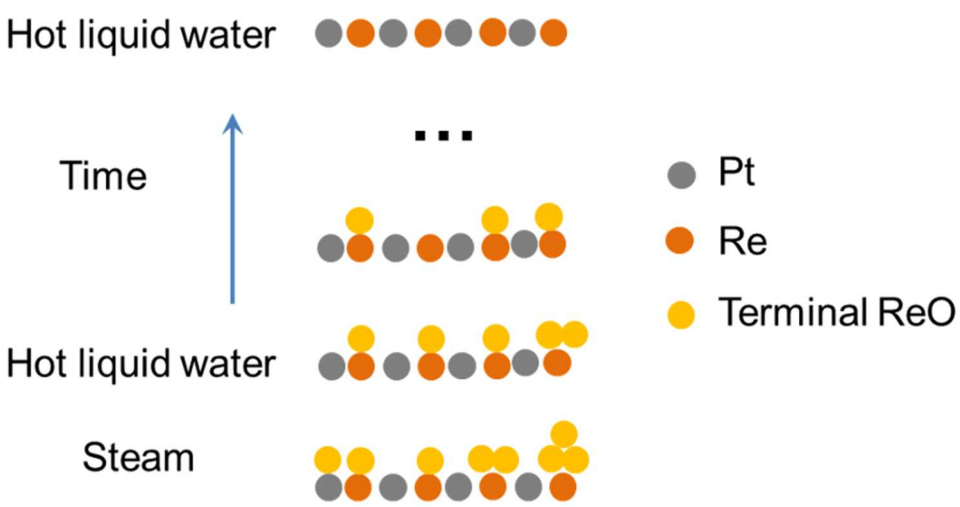

144x73mm (150 x 150 DPI)

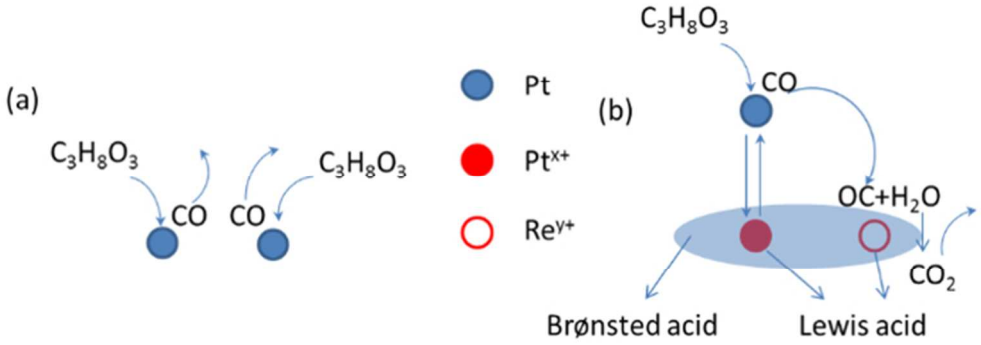

164x61mm (109 x 110 DPI)

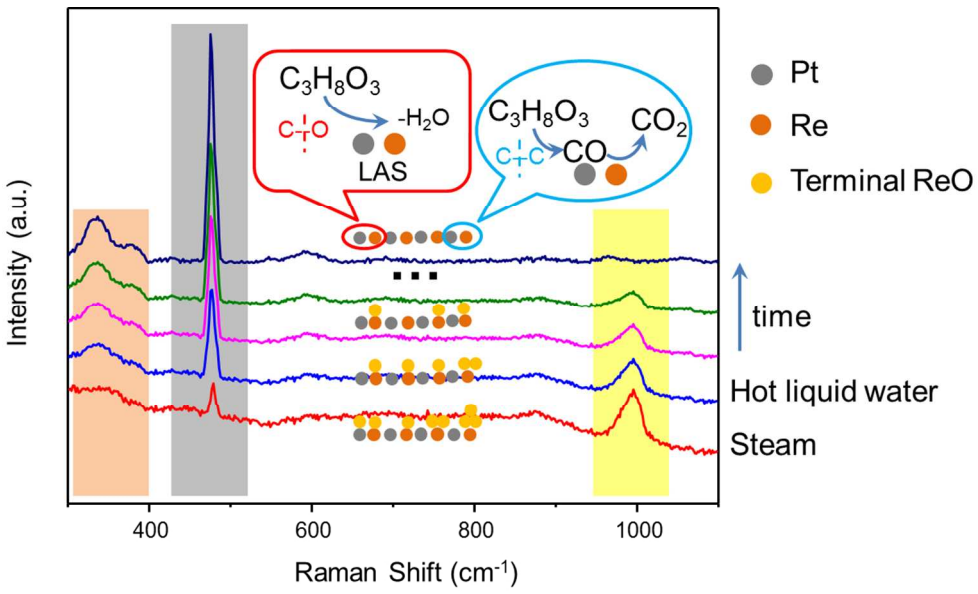

210x125mm (150 x 150 DPI)